# THE FLUCTUATING VELOCITY FIELD ABOVE THE FREE END OF A SURFACE-MOUNTED FINITE-HEIGHT SQUARE PRISM

**Rajat Chakravarty, Noorallah Rostamy, Donald J. Bergstrom and David Sumner**

Department of Mechanical Engineering
University of Saskatchewan
57 Campus Drive, Saskatoon, Saskatchewan, S7N 5A9, Canada
rajat.c@usask.ca

**ABSTRACT**

This study investigates the features of the fluctuating velocity field above the free end of a surface-mounted finite-height square prism, at a Reynolds number of Re = $4.2\times10^4$, using two state-of-the-art post-processing methodologies, namely Proper Orthogonal Decomposition (POD) and the swirling strength criterion. Instantaneous velocity measurements were obtained from Particle Image Velocimetry (PIV) experiments conducted in a low-speed wind tunnel for the flow over finite square prisms of aspect ratios AR = 9, 7, 5 and 3 (AR = $H/D$ where $H$ is the prism height and $D$ is the prism width). The prisms were immersed in a thin, turbulent boundary layer with a dimensionless thickness of $\delta/D$ = 1.6. The Reynolds number based on the freestream velocity $U_\infty$ was Re = $4.2\times10^4$. POD modes were used to extract the dominant flow features, which revealed a pair of shear sub-layers above the free end, flow entrainment from the freestream above, as well as several vortex structures in the mean shear flow region. At lower aspect ratios, the shear layers become more pronounced. Combined with the swirling strength results, this represents evidence of Kelvin-Helmholtz instabilities within the shear layer region. These instabilities increase moving away from the vertical symmetry plane. Some structures in the near wake above and behind the prism trailing edge are also seen due to the interactions of the reverse flow downstream with the downwash flow.

## INTRODUCTION

Flows over surface-mounted finite-height square prisms (of height $H$ and width $D$) have been extensively studied for related industrial applications such as buildings and electronic components on circuit boards, as well as to advance our fundamental understanding of complex turbulent wake flows. Most studies of this flow have focused on the mean flow features with lesser attention on the instantaneous flow characteristics. Furthermore, a majority of studies has concentrated on the wake characteristics of these flows with lesser attention being paid to the flow around the square prism, specifically above the free end, and its variation with aspect ratio.

The flow characteristics around and in the wake of a finite square prism have been shown to be influenced by the aspect ratio (AR = $H/D$) of the prism, the characteristics of the incoming boundary layer (thickness ratio $\delta/D$) and the Reynolds number (Re) of the flow. For both wall-mounted finite cylinder and finite square prism flows, there is a critical aspect ratio across which the wake structure shows significant change in structure. This has also been shown to affect the mean flow field above the free end of the square prism [1, 2]. Figure 1 shows the mean flow field in the vertical symmetry plane for an AR = 3 square prism. The mean flow field is characterized by flow separation from the free-end leading edge which goes on to form a separated shear layer: there is a dividing streamline which separates the freestream flow above from the recirculation zone below. Unlike the finite cylinder, this shear layer does not reattach to the free end surface of the square prism [1, 2]. Several distinct vortex structures are also observed, in particular near the trailing edge of the free end of the prism [2]. The size and location of these rotating features have all been shown to vary with aspect ratio [2]. However, the mean flow does not reveal the instantaneous turbulent structures and further analysis of the small-scale, instantaneous structures is warranted. Furthermore, identifying and characterizing rotational structures in separated shear layers by vorticity contours alone can be misleading. It is thus of interest to use more sophisticated post-processing methodologies to visualize flows in such regions of complexity which can successfully isolate rotational structures within shear layers.

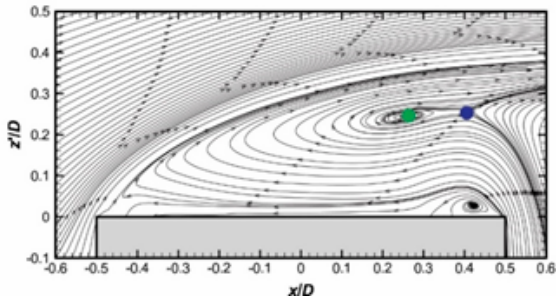


Figure 1. Mean streamlines in the vertical $x$-$z'$ symmetry plane (i.e., at cross-stream position $y/D$ = 0) above the free end of a finite square prism of AR = 3 [1, 2] (where $x$ is the streamwise coordinate and $z'$ is the vertical coordinate measured from the free-end surface). Green and blue circles denote the focus and saddle point, respectively.

## EXPERIMENTAL PROCEDURE AND POST-PROCESSING METHODS

In the present study, experiments were conducted in a low-speed wind tunnel at a Reynolds number of Re = $4.2\times10^4$ based on $D$ and the freestream velocity $U_\infty$. Finite-height square prisms of aspect ratios AR = $H/D$ = 9, 7, 5 and 3 were mounted normal to a ground plane. The relative boundary layer thickness was $\delta/D$ = 1.6. Velocity measurements were made with a two-component Particle Image Velocimetry (PIV) system in the vertical $x$-$z$ symmetry plane (at lateral position $y/D$ = 0) above the free end (where $x$ is the streamwise coordinate and $z$ is the vertical coordinate measured from the ground plane). For the AR = 3 case, velocity measurements were also made in vertical ($x$-$z$) planes at $y/D$ = 0.25 and $y/D$ = 0.375 to study the variation of the flow characteristics in the transverse direction. An ensemble of 1000 image pairs was acquired using 20 sets of 50 instantaneous snapshots. The PIV software provided a velocity vector field on a uniform mesh of 127x127 units (each unit approximately 0.015$D$ in thickness). The uncertainty in the mean velocity measurements was estimated to be about 2%. Further details are given in [1, 2].

Proper Orthogonal Decomposition analysis of the instantaneous velocity fields was performed using the snapshot method [3]. The POD methodology can be used to extract motions of different scales within the evolving dynamics of a flow, and has been used as a tool to examine wake flows [4]. The POD is applied to decompose the time-dependent fluctuating part of the flow field into an orthonormal system of spatial modes or eigenfunctions, $v_m(x)$, and associated temporal coefficients $a_m(t)$, i.e.

$$v(x_i,t) = v_o(x_i) + \sum_{m=1}^{M} a_m(t)v_m(x_i) \qquad (1)$$

Modern vortex identification schemes have also been recently developed in the literature using point-wise analysis of the velocity gradient tensor (such as the swirling strength criterion, delta criterion, second invariant, among others). The interrelationships between various schemes used are discussed in [5]. While there are considerable differences between these schemes when implemented in three-dimensional (3D) flows, local approaches to identify vortices in two-dimensional (2D) flows remain invariant to the scheme used as they all share the same principle of identifying regions where the eigenvalues of the velocity gradient tensor are complex. The swirling strength criterion [6] was used on the highest POD energy mode snapshot to visualize the vortex structures. Given that only 2D data were available, it was presumed that the regions where the 2D velocity gradient would have complex eigenvalues would be indicative of rotational vorticity.

## SELECTED RESULTS AND DISCUSSION

When applied to a set of instantaneous fluctuating velocity fields, the POD technique is able to capture regions of high energy in a flow using a finite basis of eigenmodes. Figure 2(a) shows the POD energy mode distribution as a percentage of the total energy across the various eigenmodes for the mid-plane flow above the free end of the square prism for the four aspect ratios. A higher energy distribution is seen consistently in the first two energy modes across all aspect ratios. The energy capture reaches a total of 50% of the total energy for as few as two energy modes in the AR = 9 case, increasing to 21 energy modes for the AR = 3 case. All the planes required in the range of 280-300 modes to reach 90% of the total energy. As this study was performed on the velocity fluctuation field of a flow dominated primarily by a shear layer and a recirculation zone below it [2], it was inferred that energy convergence across the eigenmodes would be more gradual owing to the presence of mainly small-scale structures along the shear layer that make a relatively small contribution to the overall energy. The temporal coefficients of the first few POD modes were analyzed, and no flow periodicity was evident. This is also consistent with an absence of a strong periodic signal in the upper wake. The energy capture in the first energy mode is lower as the aspect ratio is decreased, indicative of the fact that there are fewer but stronger coherent structures above the free end at higher aspect ratios. This may reflect that the flow field at lower aspect ratios is more strongly influenced by the ground plane [2] and the contributions of the turbulent fluctuations at smaller scales due to the ground-plane boundary layer.

Figure 2(b) shows the POD energy distribution percentage comparison for three parallel planes ($y/D$ = 0, 0.25 and 0.375) above the free end for the AR = 3 case. Once again, the first two energy modes capture considerably higher energy across the three planes. However, the energy cascade is more gradual for the planes away from the symmetry plane, each of which require at least 40 modes to reach 50% of the total energy. This indicates a weakening influence of the strongest coherent structures in the symmetry plane, owing to the influence of flow coming from the sides of the prism. It is thus of interest to also investigate the higher energy modes for the planes away from the symmetry plane to see variations in the flow characteristics of the lower energy structures.

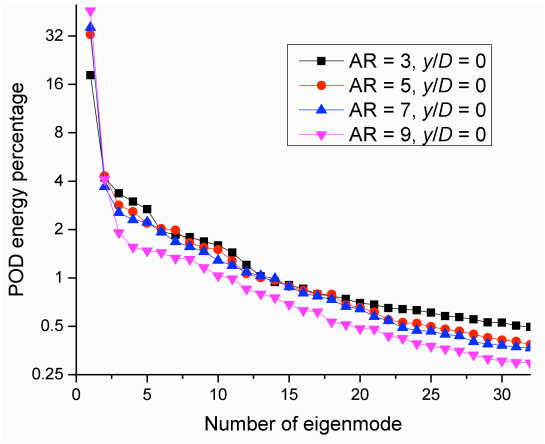


(a)

Figure 2. POD energy mode distributions: (a) for AR = 9, 7, 5 and 3 in the vertical symmetry plane ($y/D$ = 0); (b) for AR = 3 in three vertical planes.

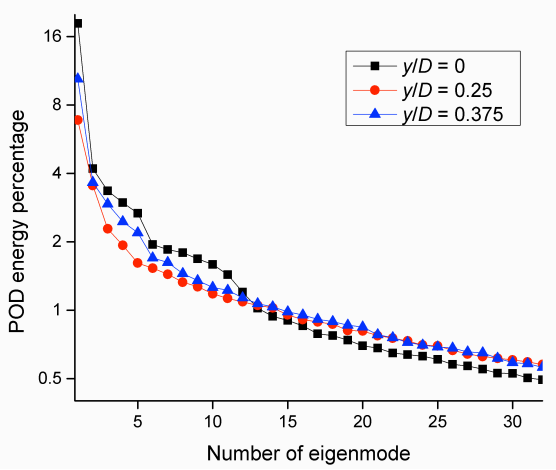


(b)

Figure 2 (continued)

**POD energy modes above the free end for AR = 3**

Figure 3 shows the $y$-vorticity contours superimposed on the 2D in-plane vector velocity field ($u$ and $w$ components) for the first, second and third mode for the vertical symmetry ($y/D$ = 0) plane. The first energy mode (Figure 3(a)) is mainly characterized by a strong shear layer coming off the leading edge of the prism and gradually diffusing into the wake without reattachment, as well as some smaller-scale structures in the upper wake above the trailing edge of the prism. This is an interesting result given that after the mean flow has been removed for the POD analysis, the energy mode reveals structures that are similar to those seen in the mean flow field. The shear layer characterizes itself as two smaller shear sub-layers of opposing vorticity at a location close to the dividing streamline observed in the mean flow field. The two sub-layers suggest a complex interaction between the separating shear layer and the recirculation zone below, similar to a mixing layer; this effect was previously observed in the separating shear layer from the forward corner of a square prism [7]. These sub-layers then become progressively weaker and degenerate into smaller turbulent structures, as seen in the higher energy modes.

To further investigate this result, the second (Figure 3(b)) and third energy mode (Figure 3(c)) are also presented. In contrast to the first mode, the second and third mode do not show the distinct shear sub-layers seen in the first energy mode. Instead, they reveal the growth of smaller structures within the shear sub-layers. The second energy mode shows some localized entrainment of flow from the freestream towards the diffusing shear layer vertically above the trailing edge of the prism. The flow field further shows the development of a rotational vortex structure due to the interactions between the shear layer and the entraining fluid from the freestream above. The small-scale structures likely represent Kelvin-Helmholtz (KH) instabilities, previously observed within the shear flows separating around surface-mounted cylinders for a similar Reynolds number [8]. The external perturbations responsible for these instabilities may originate from the incoming turbulent boundary layer (the boundary layer on the ground plane is proportionally thicker for the prism of AR = 3). As both these layers extend downstream, the regions of different momentum interact with each other. The associated instabilities grow in size and are deformed by the three-dimensional influence of the surrounding turbulent flow. In addition, the third mode also shows the growth of a rotational clockwise vortex just downstream of the trailing edge as seen in the mean flow [1, 2]. This specific vortex structure is not seen in any of the first three energy modes at higher aspect ratios (not shown), indicating that the AR = 3 prism has the strongest upward-directed flow from the ground plane that contributes to the formation of these structures in the instantaneous field. In previous studies of the mean flow field, this rotational structure, termed vortex $B_t$, has appeared across all aspect ratios, but is largest in size for the prism of AR = 3 [2].

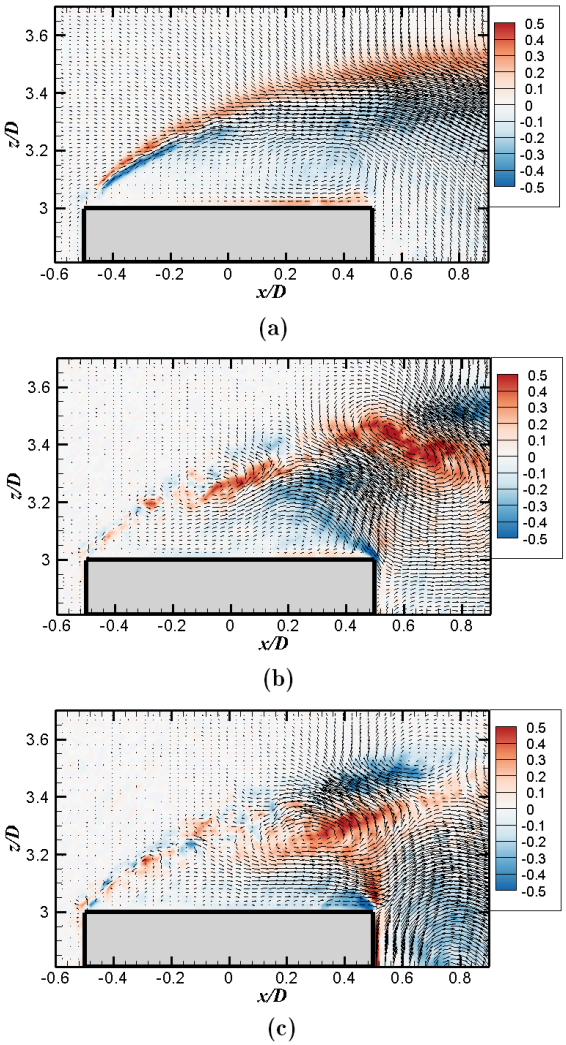


(a)

(b)

(c)

Figure 3. 2D velocity vector field above the free end, in the vertical symmetry plane ($y/D$ = 0), along with $y$-vorticity contours, for the (a) first, (b) second and (c) third modes, for the finite square prism of AR = 3.

Figure 4 shows the $y$-vorticity contours superimposed on the 2D in-plane vector velocity field for the fourth energy mode for the vertical planes at $y/D$ = 0 and $y/D$ =

0.375. On the symmetry plane ($y/D$ = 0), the smaller structures in the shear layer appear more stretched along the location of the dividing streamline in the mean flow. These then go on to form larger counter-rotating vortex structures due to similar interactions seen in the lower energy modes. In contrast, the fourth energy mode in the $y/D$ = 0.375 plane shows much smaller structures along the dividing streamline likely indicating a higher level of KH-instabilities in planes moving away from the symmetry plane due to entrainment of fluid coming at different velocities from the sides of the prism. There is also evidence of a clockwise vortex structure above the trailing edge of the free end in the $y/D$ = 0.375 plane. The height above the free end at which this structure appears for the $y/D$ = 0.375 plane is also higher than for the symmetry plane. There is also no pronounced reverse flow seen in the $y/D$ = 0.375 plane in the near wake suggesting the more prominent influence of momentum from the freestream flow from the sides of the prism.

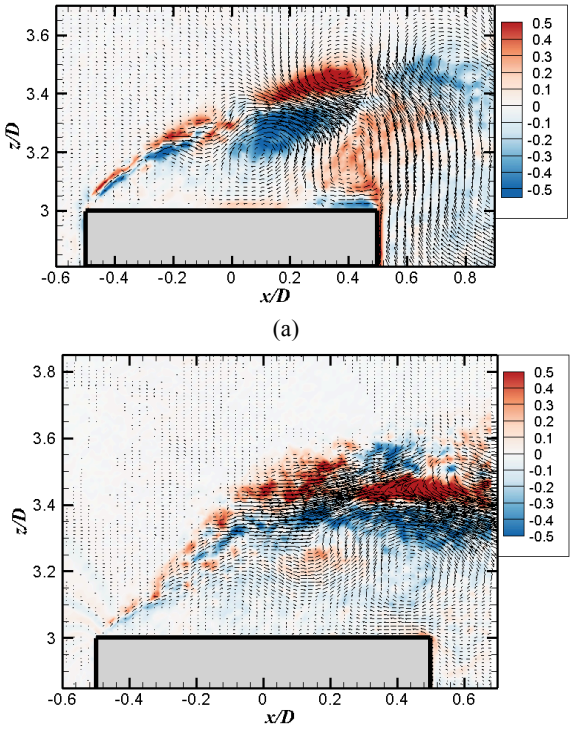


(a)

(b)

Figure 4. 2D velocity vector field above the free end, along with $y$-vorticity contours, for the fourth energy mode, in vertical planes at (a) $y/D$ = 0 and (b) $y/D$ = 0.375, for the finite square prism of AR = 3.

## POD energy modes at higher AR

For the prisms of higher AR, the first POD energy mode in the symmetry plane above the free end shows almost similar characteristics with the AR = 3 case. Two examples for AR = 5 and 9 are shown in Figure 5(a) and 5(b), respectively. Once again, a distinct pair of shear sub-layers in the vicinity of the dividing streamline of the mean flow is observed. Vorticity in the shear sub-layers is strongest just beyond the prism leading edge and once again becomes progressively weaker downstream. The thickness of the recirculation zone is seen to reduce with increasing aspect ratio. The small vortical structure near the trailing edge evident in the AR = 3 flow (Figure 3(a)) is also witnessed in the AR = 5 flow (Figure 5(a)), but is weaker. This structure is not seen for the prisms of AR = 7 and AR = 9 indicating that the structure is perhaps an artefact of the strength of the recirculation zone above the free end of the prism, which simultaneously gets weaker with increasing aspect ratio. Downstream of the prism, just after the trailing edge of the free end, the flow becomes stronger with increasing aspect ratio. This may be attributed to the reduction in size of mean vortex $B_t$ in the upper part of the near wake [2] with increasing aspect ratio. The formation of the smaller vortex structure just above the trailing edge of the prism seen in the mean flow is not seen in any of the first POD energy modes, indicating that it may have been filtered out with the mean flow.

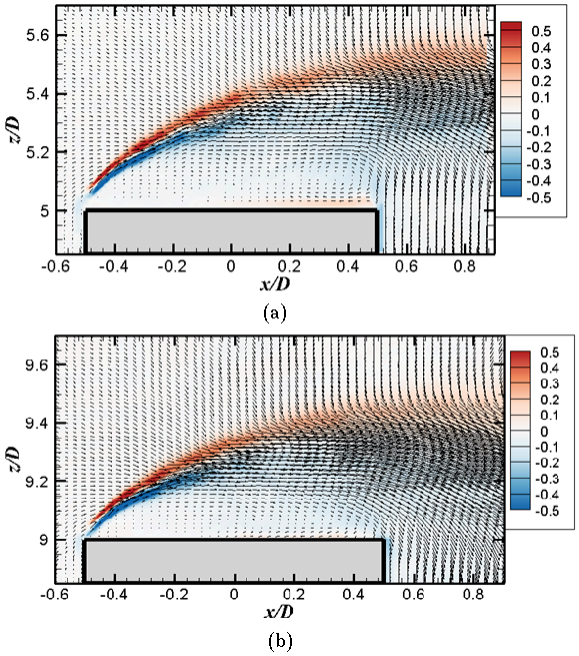


(a)

(b)

Figure 5. 2D velocity vector field above the free end, in the vertical symmetry plane ($y/D$ = 0), along with $y$-vorticity contours, for the first energy mode for the prisms of (a) AR = 5 and (b) AR = 9.

The second POD energy mode across the higher aspect ratios (not shown) also reveals the strong shear sub-layers seen in the first POD energy mode. Figure 6 shows the third energy mode in the vertical symmetry plane for AR = 5, 7 and 9. Once again, similar shear-layer instabilities are observed. An interesting observation is that the tendency for formation of these shear-layer instabilities reduces with increasing aspect ratio. Figure 6(a), for AR = 5, already shows a reduced number of vortex structures compared to the AR = 3 case (Figure 3(c)), and this number progressively reduces until the AR = 9 case (Figure 6(c)), where only a couple of weakly rotating structures are observed and entrainment across the shear sub-layers stops a short distance after the leading edge of the prism. This is suggestive of the fact that with increasing aspect ratio, the velocity disparity between the shear layer from the leading edge and the surrounding freestream flow is further reduced thereby creating fewer

instabilities. The entrainment of fluid across the shear sub-layers is thus a strong function of the aspect ratio, and may be influenced by effects of the ground plane and/or the boundary layer.

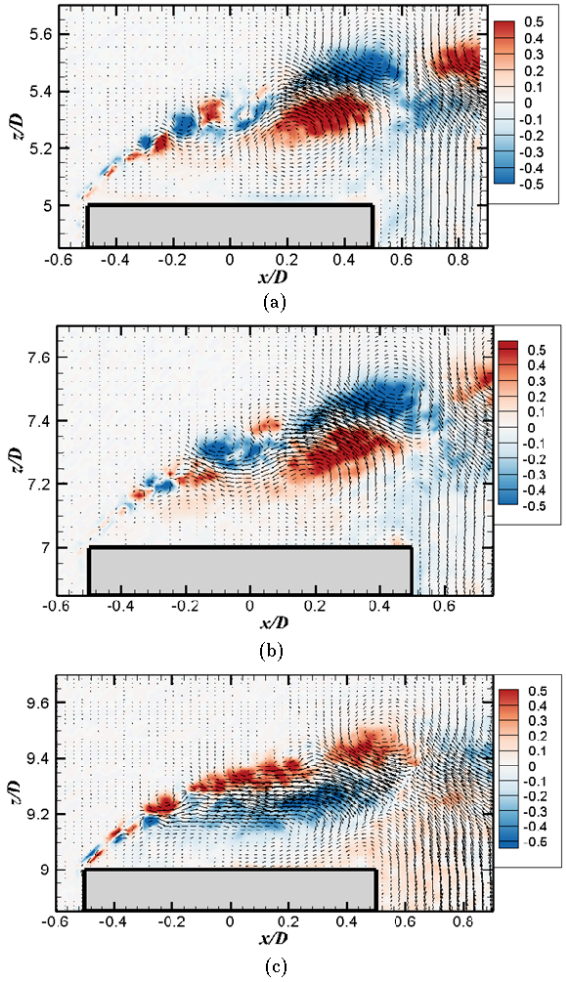


Figure 6. 2D velocity vector field above the free end, in the vertical symmetry plane ($y/D = 0$), along with $y$-vorticity contours, for the third energy mode for the prisms of (a) AR = 5, (b) AR = 7, and (c) AR = 9.

## Swirling Strength Results

The primary advantage of swirling strength is its capability of isolating rotational vorticity in the $y$-vorticity contour plots (thereby selectively filtering out the vorticity solely due to shear). This is particularly useful in decomposing shear flows into their constituent vortex structures. Figure 7 shows the application of the swirling strength criterion on the first and third POD energy modes for the vertical symmetry plane above the prism of AR = 3. The vectors have been shown with an index skip of two nodes for better clarity of the swirling strength criterion in all the following figures. In 2D, despite the inherent limitation of not being able to predict the rotational orientation of these vortex structures, swirling strength shows remarkable correspondence with the flow field characteristics exhibited by both the mean flow field and the POD energy mode results. An example of this is the swirling strength contour strongly visible at the clockwise rotational vortex in Figure 7(b). It shows how the beginning of the shear layer is composed of strong vortices, which on further interaction with the outer flow and the recirculation zone below it, smear into weaker structures downstream. Swirling strength is able to identify some relatively strong small-scale vortex structures even in regions of weaker $y$-vorticity. Furthermore, swirling strength is successful in revealing vortices at a higher resolution that are difficult to visualize from the vector profiles owing to the small size (magnitude) of the vectors in the recirculation zone of the instantaneous field. Thus, if applied in tandem on 2D flow fields, POD can be used to predict the presence and sign of vorticity in a velocity field, and the swirling strength criterion can be used to resolve this vorticity as a rotational motion.

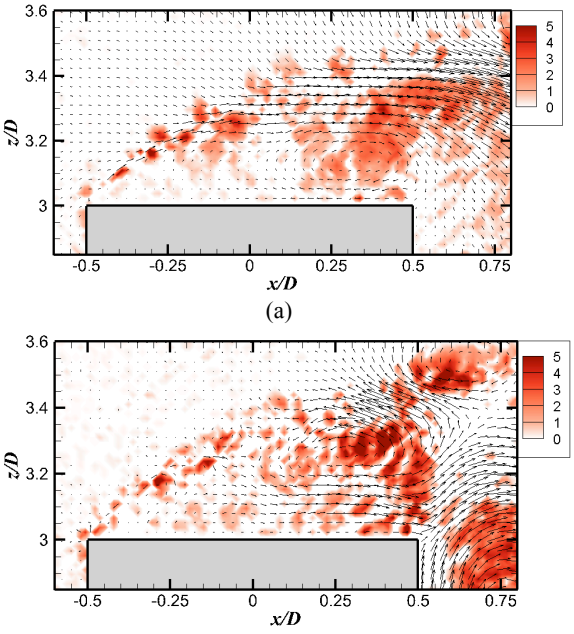


Figure 7. 2D velocity vector field above the free end, in the vertical symmetry plane ($y/D = 0$) for the prism of AR = 3, for the (a) first energy mode, and the (b) third energy mode.

Figure 8 shows the swirling strength contours for the first energy mode in the vertical symmetry plane above the free end for the AR = 5, 7 and 9 square prisms, respectively. In all cases, strong vortices separating from the leading edge are seen smearing into the wake, similar to those seen for the AR = 3 free end. As aspect ratio increases, these rotational structures reduce in strength and number, and are only observed closer to the leading edge of the prism. The height above the free end where these structures are seen also reduces with increasing aspect ratio and the rotational structures appear to become more elongated. These features indicate that moving away from the ground plane increases the influence of diffusion from the freestream flow above in smearing the wake above the free end. This is also supported by the velocity vectors which show a stronger alignment and earlier onset of flow in the freestream direction above the free end in

this separating layer of vortex structures as the aspect ratio increases.

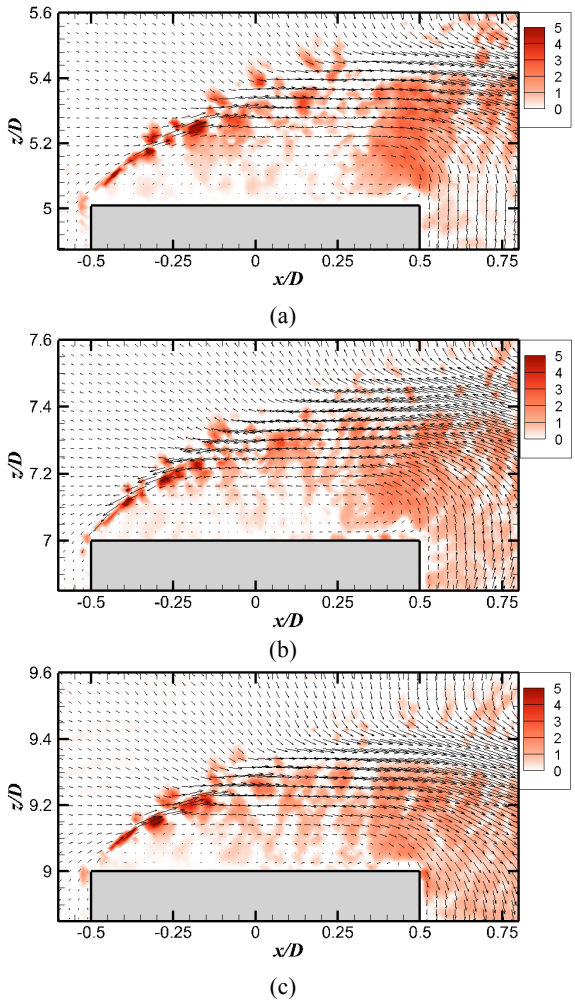


Figure 8. Swirling strength contours in the vertical symmetry plane ($y/D = 0$) above the free end of the prism, along with the 2D velocity vectors for the first energy mode for (a) AR = 5, (b) AR = 7, and (b) AR = 9.

## CONCLUSIONS

The objective of this study was to investigate the fluctuating flow field above the free end of a surface-mounted finite-height square prism using POD and the swirling strength criterion. Data for the flow visualization methodologies were obtained from experiments conducted in a low-speed wind tunnel using PIV. The mean flow field [2] remained largely similar across all aspect ratios with a shear layer of flow separation originating from the leading edge of the prism, a recirculation zone beneath this shear layer, and a saddle point downstream at the end of the recirculation zone [2].

In all the vertical planes, the first POD energy mode characterized the shear layer separating from the leading edge of the prism as consisting of two distinct shear sub-layers of clockwise and counter-clockwise vorticity, formed due to opposing interactions with the recirculation zone below and the freestream outer flow above. With an increase in aspect ratio, the recirculation zone and the height of the shear layer become progressively thinner. The higher POD modes further characterised these sub-layers as containing distinct small-scale vortices. These vortices were strong near the leading edge, but became progressively weaker moving downstream. As the shear layer progressed into the wake, turbulent fluxes lead to localized entrainment of flow across the interface of the shear sub-layers. These are evidence of Kelvin-Helmholtz instabilities seen in similar flows at these Reynolds numbers at the boundary of two different fluid layers moving at different velocities. At higher aspect ratios, the tendency for the formation of these instabilities reduced, possibly due to the weaker influence of the ground plane. However, these instabilities become more enhanced moving away from the symmetry plane due to the influence of fluid momentum from the sides of the prism.

To characterize this shear layer of vorticity into distinct rotational vorticity, the swirling strength criterion was used. For various modes, the swirling strength criterion characterized this shear layer as the shedding of rotational vortices detaching from the leading edge of the prism along the shear layer, confirmed previously by the second and third POD energy modes. Swirling strength was able to further resolve a higher energy mode into smaller vortex structures. Swirling strength was thus able to capture added information on rotational vortices over and above the POD vorticity contours.

## REFERENCES


[1] Rostamy, N., D. Sumner, D. J. Bergstrom and J. D. Bugg, 2013, Instantaneous flow field above the free end of finite-height cylinders and prisms, *International Journal of Heat and Fluid Flow*, **43**: 120-128.

[2] Sumner, D., N. Rostamy, D. J. Bergstrom, and J. D. Bugg, 2017, Influence of aspect ratio on the mean flow field of a surface-mounted finite-height square prism, *International Journal of Heat and Fluid Flow*, **65**: 1-20.

[3] Sirovich, L., 1987, Method of snapshots, *Q. Appl. Math,* **45**: 561-571.

[4] Wang, H. F., H. L. Cao, and Y. Zhou, 2014, POD analysis of a finite-length cylinder near wake. *Experiments in Fluids*, **55(8)**, 1790-1804.

[5] Chakraborty, P., S. Balachandar, and R. J. Adrian, 2005, On the relationships between local vortex identification schemes, *Journal of Fluid Mechanics*, **535**: 189-214.

[6] Chong, M. S., A. E. Perry and B. J. Cantwell, 1990, A general classification of three-dimensional flow fields, *Physics of Fluids A: Fluid Dynamics* **2.5**: 765-777.

[7] Lyn, D. A. and W. Rodi, 1994, The flapping shear layer formed by flow separation from the forward corner of a square cylinder. *Journal of Fluid Mechanics*, **267**: 353-376.

[8] Hain, R., C. J. Kähler and D. Michaelis, 2008, Tomographic and time resolved PIV measurements on a finite cylinder mounted on a flat plate. *Experiments in Fluids*, **45(4)**, 715-724.